Correlated Structural and Luminescence Analysis of B-Doped Si-Nanocrystals Embedded in Silica

Rémi Demoulin, Dominique Muller, Daniel Mathiot, Philippe Pareige, Etienne Talbot

Correlated Structural and Luminescence Analysis of B-Doped Si-Nanocrystals Embedded in Silica

*Rémi Demoulin, Dominique Muller, Daniel Mathiot, Philippe Pareige, and Etienne Talbot**

Structural characteristics and luminescence properties of B-doped silicon nanocrystals (Si-ncs) embedded in a SiO_2 matrix elaborated by ion beam synthesis are investigated. The use of atom probe tomography gives a unique opportunity to experimentally evidence the exact location and composition of B atoms in doped Si-ncs. These experiments allow to conclude about a favored B location at the periphery of the Si-ncs depending on their size. In this way, two categories of Si-ncs can be described: 1) largest Si-ncs that are B-doped and where B atoms are located at the Si-ncs/SiO_2 interface, and 2) smallest Si-ncs that remain undoped but seem to be surrounded by a B-rich SiO_2 shell. These structural characteristics (composition and diameters) are correlated to the photoluminescence properties of these Si-ncs. These measurements show the well-known quenching of Si-ncs luminescence due to high B doping, which allows us to conclude about the environment changes brought by the presence of B in Si-ncs or of B-rich shell around Si-ncs.

Due to quantum confinement, by controlling the shape and the size of silicon nanocrystals (Si-ncs), properties of materials consisting of Si-ncs embedded in SiO_2 can be tuned to develop microelectronic or optoelectronic devices[1,2]. Another way to modify the properties of these materials consists in the introduction of n or p-type impurities in Si-ncs, by the process of doping.[3,4] For instance, it has been demonstrated that a high doping level in Si-ncs may lead to the appearance of new plasmonic properties.[5,6] A precise control of the impurity level in these Si nanostructures allows the tuning of these properties for a specific application.[7] However, the properties of doped materials also seem to be closely linked to their nanostructures and especially to the precise location of the impurities (i.e., in the core of Si-ncs, at the Si-ncs interface, or in the surrounding matrix). These last years a strong interest has been paid on optical, electrical, and recently on plasmonic properties. However, investigations on structural properties of doped Si-ncs are not numerous. Recently, we have performed a deep structural analysis, at the atomic scale, of n-type doping in Si-ncs embedded in SiO_2, using atom probe tomography (APT).[8] The growth of Si-ncs and their doping were achieved by the coimplantation of Si and As or P in a SiO_2 layer. These investigations allowed us to conclude that a high level of As or P (5–40 at%) can be introduced in the core of Si-ncs. Considering the p-type doping of Si-ncs embedded in SiO_2, theoretical calculations have demonstrated that the energy required to remove a B atom from the Si-nc core is much lower than for a P atom.[9] This makes the diffusion of B atoms toward SiO_2 easier and it should induce a favored location of these impurities in the SiO_2 phase, as in the case of Si bulk materials.[10] By consequence, from an experimental point of view, Hiller et al. have shown that B doping of Si-ncs can be hardly performed by plasma-enhanced chemical vapor deposition (PECVD).[11] In this case, only a minority of Si-ncs are doped and contain less than two impurities that may be located at the Si/SiO_2 interfaces. In this article, we propose to investigate the compositions of B-doped Si-ncs embedded in SiO_2 thin layer, elaborated by ion beam synthesis. The use of APT process allowed us to define the composition of the nanostructure of the sample and to determine the precise location of B atoms regarding Si-ncs.

Figure 1 shows the 3D reconstruction of the ^{29}Si and ^{11}B coimplanted SiO_2 thin layer. The 3D mapping of Si atoms (Figure 1a) evidenced the formation of Si-ncs in the implantation range of ^{29}Si after an annealing at 1100 °C. Concerning B distribution (Figure 1b), in this view, it seems difficult to define a favored location with respect to the Si-ncs. However, by applying the first nearest neighbor principle,[12] we have estimated that only 20% of B atoms are located near to the Si clusters positions. The remaining 80% are diluted in the SiO_2 matrix, which corresponds to an impurity composition of 4.2×10^{20} at.cm^{-3}. The solubility of B in SiO_2 is higher than the solubility limit usually measured in pure Si (2×10^{20} at.cm^{-3}). Considering the solubility of B in Si and SiO_2, the segregation coefficient at the Si-nc/SiO_2 interface is estimated at 0.48. This value is consistent with the result obtained at bulk Si/SiO_2 interface

Dr. R. Demoulin, Prof. P. Pareige, Dr. E. Talbot
UNIROUEN
INSA Rouen
CNRS
Groupe de Physique des Matériaux
Normandie Univ
76000 Rouen, France
E-mail: etienne.talbot@univ-rouen.fr
Dr. D. Muller, Prof. D. Mathiot
Cube Laboratory
Université de Strasbourg and CNRS
B.P. 20, 67037 Strasbourg cedex, France

DOI: 10.1002/pssr.202000107

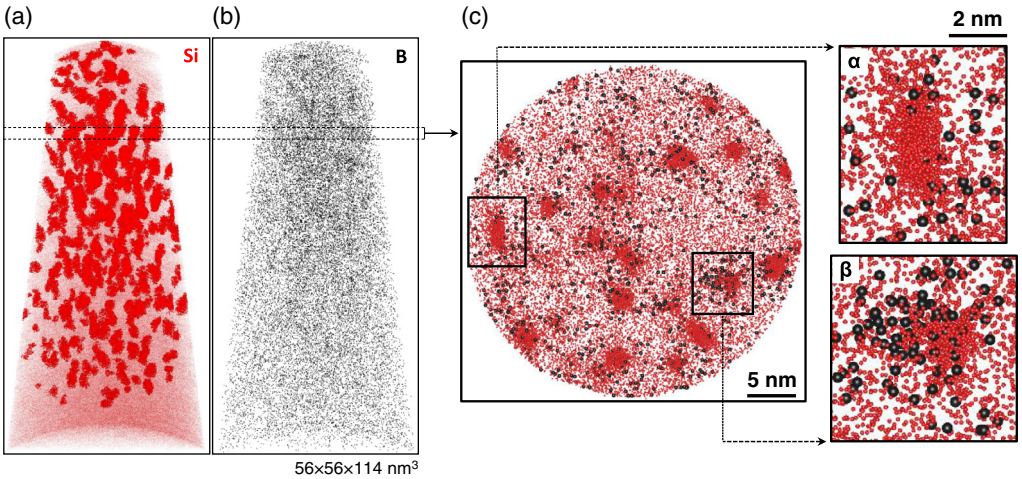

Figure 1. a) Distribution of Si atoms with a highlighting of Si-ncs and b) distribution of B atoms in ^{29}Si and ^{11}B coimplanted SiO_2 thin layer. c) Cross-section extracted from the analyzed volume near to the implantation peak. Red and black dots correspond to Si and B atoms, respectively. The volume is $35 \times 35 \times 3$ nm^3. Regions α and β represent two magnified views of an undoped Si-nc and a B-doped Si-nc.

(0.3–0.5).[10,13] To examine closely the location of B, Figure 1c represents the atomic distributions of Si and B in a cross-section extracted from the analyzed volume near to the implantation peak. It allows describing different types of Si-ncs. On one hand, region α highlights that some Si-ncs should not contain any B atoms or only at their surface. In contrast, region β evidenced an aggregation of B atoms around a Si-nc. Thereafter, we will consider two types of Si-ncs that may coexist in a single thin layer, noted undoped Si-ncs and B-doped Si-ncs.

The size distributions of the Si-ncs in undoped and B-doped samples are plotted in **Figure 2**a. It is worth noting that in both samples, the size distributions are quite similar, following the same evolution in a lognormal shape, and with almost equal mean diameter, estimated at 2.5 nm ($\sigma = 0.6$ nm) in the undoped layer and 2.6 nm ($\sigma = 0.7$ nm) in the B-doped layer. Some studies reveal that the introduction of impurities could modify the growth characteristics of Si-ncs.[14,15] In a recent work, using similar elaboration conditions, we have demonstrated that in the presence of P atoms, the size of Si-ncs increases, reaching a mean diameter of 3.3 nm ($\sigma = 1.0$ nm).[8] Here, the introduction of B atoms does not seem to influence the growth of Si-ncs. In the B-doped sample, the composition of each Si-ncs have been corrected from local magnification effect.[16] In fact, during APT experiments, due to the high difference of evaporation field required to trigger the evaporation of the different phases, elements from the SiO_2 matrix can be artificially introduced in the Si-ncs and must be identified. Moreover, the background noise of the mass spectrum must be estimated. In this way, to consider the limits of the detection system (10^{18} at cm^{-3}), here, we considered that a Si-nc is B-doped only if more than 5 B events are detected in the nanostructure. This means that the quantity of B-doped Si-ncs may be slightly underestimated.

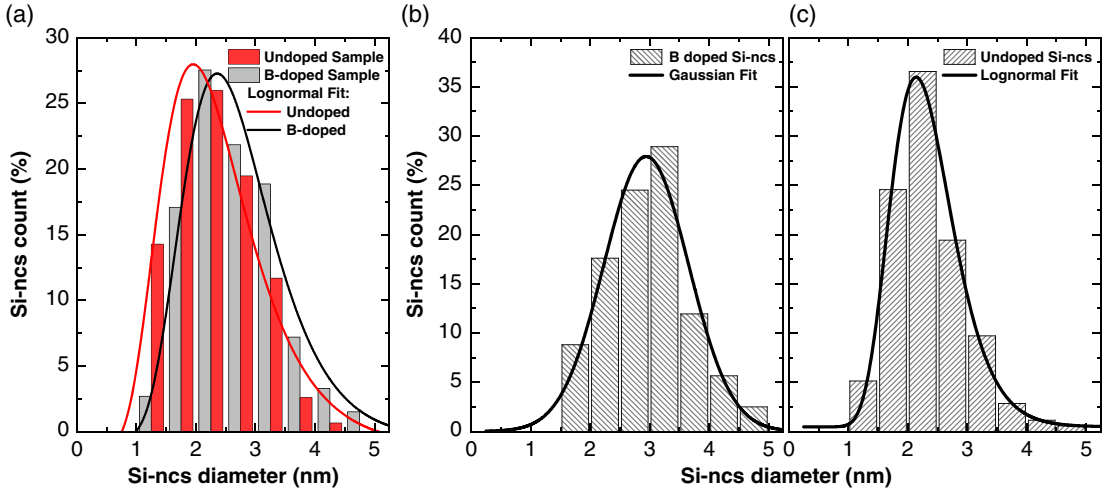

Figure 2. a) Comparison between size distributions of all Si-ncs measured in undoped (red) and B-doped (gray) thin layers. Size distributions of b) B-doped and c) undoped Si-ncs population observed in the B-doped thin layer.

In this case, it appeared that among the 334 Si-ncs detected in the entire volume (Figure 1a), only 48% contain at least one B atom. Regarding this, the size distribution of Si-ncs of B-doped thin layer has been separated in two part, by considering B-doped (Figure 2b) and undoped Si-ncs (Figure 2c). Mean diameters are respectively estimated at 3.0 nm ($\sigma = 0.7$ nm) for B-doped and 2.3 nm ($\sigma = 0.6$ nm) for undoped Si-ncs. It allowed us to evidence a clear difference of mean diameter between both types of Si-ncs, and it reveals a strong influence of the Si-ncs size on their doping. In fact, undoped Si-ncs follow the same characteristics as observed for Si-ncs of undoped sample, but B-doped Si-ncs show a different size distribution shape and larger diameters. This may indicate that the probability to insert B atoms in a Si-nc increases when its size increases.

In addition to the characterization of atomic distributions and size distributions of Si-ncs, APT analyses bring a unique opportunity to define experimentally the precise location of impurities around Si-ncs. **Figure 3**a,c represent the erosion profiles computed for B-doped and undoped Si-ncs. An erosion profile describes the evolution of the composition of each species from the center to the surrounding matrix of clusters. The establishment of these profiles relies on both envelope and erosion methods.[17] In the first step, an envelope is defined around the Si cluster. Then, atoms are removed step by step from its surface. Finally, the erosion profile can be plotted by computing the composition of the eroded Si cluster at each step of the erosion. In this kind of sample, the detection of oxygen atoms in Si-ncs is the consequence of the local magnification effect. Then, raw compositions measured for B erosion profiles may be underestimated near Si-ncs.

In the case of B-doped Si-ncs, the composition of B reaches its maximum (1.0 at%) at the Si-nc/SiO_2 interface and decreases in the core of Si-ncs. After correction, the B composition measured in B-doped Si-ncs are lower than 2 at% for about 85% of Si-ncs. As shown in Figure 3b, these observations on erosion profiles evidenced a favored location of B atoms on both sides of the Si-nc/SiO_2 interface. Concerning the case of undoped Si-ncs, B composition slightly increases from 0.5 to 0.6 at%, in the SiO_2 matrix near to the Si-ncs surface and abruptly decreases in the core of Si-ncs. The measurement of a low B composition in the Si-ncs is due to noise detection and size dispersion of undoped Si-ncs; no B atoms are located in these Si-ncs. This may indicate that even in undoped Si-ncs, B atoms tend to accumulate near to the Si-ncs/SiO_2 interface. As shown in Figure 3d, this phenomenon should be schematized by the presence of an intermediate shell between Si-ncs and SiO_2 matrix that contains a larger amount of B atoms than the rest of the matrix. Considering the formation of a B-rich SiO_2 shell of 0.5 nm around Si-ncs and considering the size dispersion of undoped Si-ncs (Figure 2c), it may represent a quantity of 4–10 B atoms in the intermediate shell.

It is worth noting that this experimental observation of a B aggregation at the Si-nc/SiO_2 interface is consistent with theoretical computation lead on B-doped Si-ncs embedded in SiO_2.[9,18,19] Moreover, it confirms the recent experimental investigation of Hiller et al. based on a PECVD elaboration.[11] It is also consistent with recent work based on other investigation method. In fact, by combining X-ray diffraction experiments with Monte Carlo simulation, Hunter et al. have evidenced the location of B at the Si-ncs surface in Si-ncs of barely 5 nm of diameter doped with 2.5–10% B.[20] This particular location of B atoms in the periphery of Si-ncs may be explained by different phenomena. First, theoretical studies have shown that the positioning of B atoms at interfacial sites is energetically favored.[9,19] Second, as the solubility of B in SiO_2 is higher than in Si, the diffusion of B atoms toward the Si-nc/SiO_2 interface to settle in the matrix can be expected. Then, if the solubility limit of B in SiO_2 is reached, due to the low solubility of B in Si, the excess of B should be trapped at the periphery of the Si-ncs. Finally, the aggregation of B atoms at the Si-nc/SiO_2 interface of the largest Si-ncs and the presence of a B-rich SiO_2 shell around the smallest ones may be also the result of the self-purification effect, which tends to expel the impurities from the Si-ncs.[21]

Additional investigations have been performed on photoluminescence (PL) properties. **Figure 4** represents the PL spectra of undoped and B-doped thin layers in function of the dose of

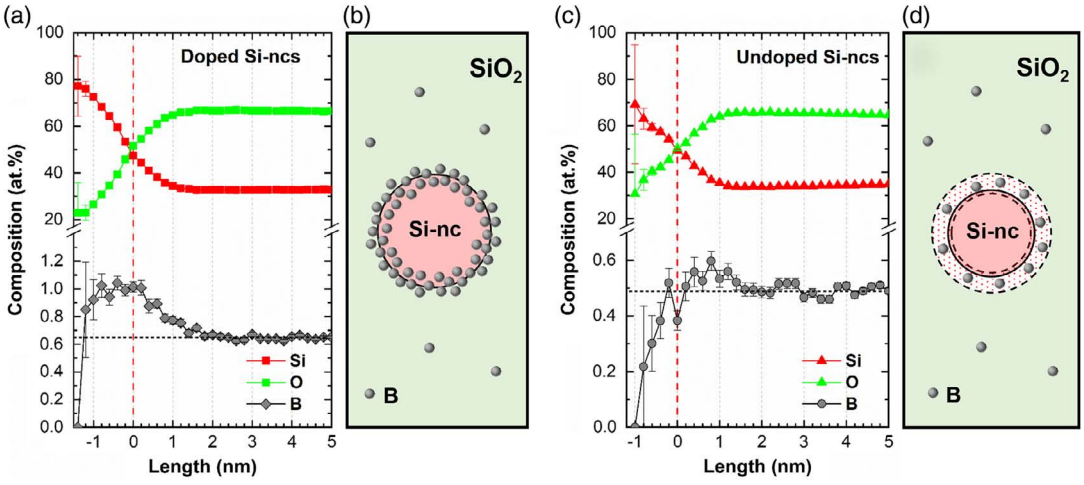

Figure 3. Mean erosion profiles of a) B-doped and c) undoped Si-ncs. The zero position corresponds to the Si-nc/SiO_2 interface. b,d) Corresponding illustrations of B positioning around a Si-nc embedded in SiO_2 for each case.

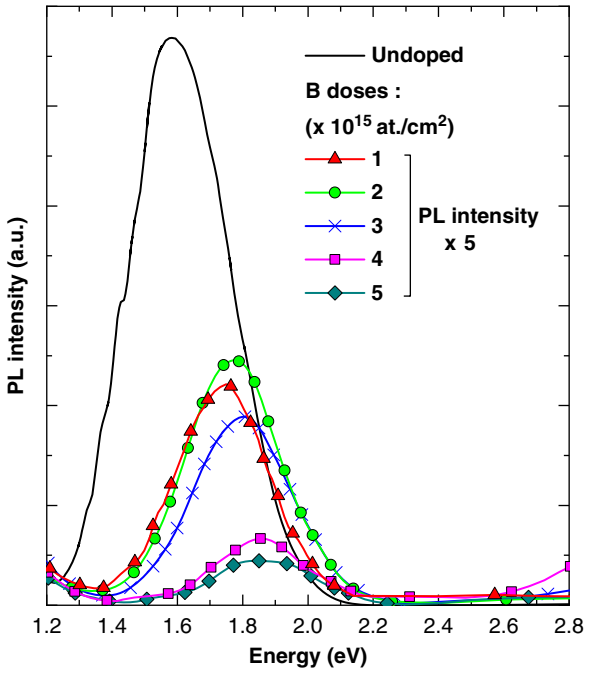

Figure 4. PL spectra of Si and B coimplanted SiO_2 thin layer annealed at 1100 °C in function of the B-implanted dose. The PL intensity of B-doped layers are magnified by a factor of 5.

implanted B. The PL band centered at 1.6 eV, observed in undoped sample, should originate from the recombination of electron–hole pair in Si-ncs. As shown in Figure 2a for the highest dose of B (5×10^{15} at.cm^{-2}), the presence of B atoms does not have influence on the growth of Si-ncs; however, it seems to have a strong impact on their PL properties even for the lowest doses. Two observations can be extracted from these PL measurements. First, it highlights that the B implantation results in a strong decrease in the Si-ncs PL intensity, even for the lowest doses. Second, an increase in the B dose induces a blue shift of the PL band from 1.6 eV in the undoped layer to 1.9 eV for a B dose of 5×10^{15} at.cm^{-2}.

Both of these effects on PL luminescence of B-doped Si-ncs agree with the observations of other authors whether for the case of freestanding Si-ncs or Si-ncs embedded in SiO_2 matrix.[11,22–26] APT analyses evidenced that B atoms are only detected in the biggest Si-ncs. As the presence of a single B atom may lead to the deactivation of the Si-nc, we can assume that only the smallest Si-ncs exhibit a PL signal. This observation may explain the blueshift of the PL band observed on B-doped samples. This should be attributed to the higher doping formation energy required to perform the doping of the smallest Si structures and to a greater influence of the self-purification effect which tends to keep these nanostructures undoped.[21,27] The origin of the decrease in the PL signal intensity seems much more complicated. In the case of the B-doped Si-ncs embedded in SiO_2 matrix, the quenching of the PL signal is a well-known effect and is often attributed to the Auger recombination process or strain-induced defect states.[14,22,28] In our case, for the highest dose, APT analyses have clearly shown the location of B atoms at the Si-nc/SiO_2 interface of a part of Si-ncs, which can confirm the effect of these nonradiative recombination processes. However, only 48% of Si-ncs contain B atoms. Then, the 52% of Si-ncs that still undoped should contribute to the PL, so we could expect to measure PL signal with a higher PL intensity. Also, for lower B doses, as the fraction of undoped Si-ncs may be more important, the PL signal may be more intense. But, for B doses from 1 to 3×10^{15} at.cm^{-2}, PL intensities are barely equal. It means that B atoms present in the SiO_2 matrix, especially near to the Si-ncs, can interact with Si-ncs and modify their properties. In fact, for free-standing Si-ncs, it has been evidenced that the modification of the Si-ncs surface can generate a change in their electronic structure and then influence their optical properties.[29,30] Here, concerning undoped Si-ncs, Figure 3c,d demonstrate the presence of B-rich SiO_2 shell surrounding the Si-ncs. The formation of this shell may locally change the environment of Si-ncs by introducing defect states, acting as nonradiative recombination centers, such as oxygen dangling bonds or length distortions due to the lower radius of B atoms.[9,23,31]

In summary, the compositions of B-doped Si-ncs embedded in SiO_2 elaborated by ion beam synthesis have been investigated. It was evidenced that only the largest Si-ncs are B-doped, and that impurities are mainly located at the Si-ncs/SiO_2 interfaces. However, smallest Si-ncs, which still undoped, also seem to be influenced by the B doping. Indeed, the formation of a B-rich SiO_2 shell surrounding these undoped Si-ncs was highlighted. The presence of this B-rich SiO_2 shell induces a modification of the Si-ncs environment leading to a quenching of their luminescence properties.

Experimental Section

Undoped and boron-doped thin layers were prepared using ion beam synthesis process. An isotopically pure silicon (^{28}Si) wafer was oxidized to form a 200 nm thick $^{28}SiO_2$ layer. Then, the samples were implanted with ^{29}Si at 50 keV at a dose of 6×10^{16} cm^{-2}. For the B-doped sample, to match with the projection range of ^{29}Si, ^{11}B was implanted at 17 keV at a dose of 5×10^{15} cm^{-2}. Finally, the thin films were annealed at 1100 °C for 4 h in pure N_2 to form Si-ncs and for impurities diffusion. According to these parameters, the composition of implanted species reaches a maximum of 10.6 at% for ^{29}Si and 1.2 at% for ^{11}B at the implantation peak. The 3D atomic scale characterization of B-doped thin layer was carried out using a laser-assisted wide-angle tomographic atom probe (LAWATAP, Cameca) with a femtosecond UV pulsed laser (350 fs, 33 nJ, $\lambda = 343$ nm) and a detector yield of 0.62. APT process is based on the evaporation field effect applied on surface atoms of a sharp tip with a curvature radius lower than 50 nm. The preparation of sharp tips was achieved by using the lift out and annular milling procedure,[32] using a ThermoScientific plasma FIB Hélios G4 CXe. Data analysis was performed using GPM3Dsoft software. For this sample, the 3D reconstruction was based on a scanning electron microscopy (SEM) picture of the tip observed before APT analysis to estimate the curvature radius.[17] Complete 3D reconstructions of both samples and corresponding composition profiles of implanted species are shown in Figure S1 to S4, Supporting Information. PL spectra were measured with an excitation wavelength of 355 nm. Earlier, a second annealing at 450 °C for 20 min (90% N_2 + 10% H_2) was performed to passivate the nonradiative interface defects.

Supporting Information

Supporting Information is available from the Wiley Online Library or from the author.

[1] D. V. Talapin, J. S. Lee, M. V. Kovalenko, E. V. Shevchenko, *Chem. Rev.* **2010**, *110*, 389.

[2] L. Khriachtchev, S. Ossicini, F. Iacona, F. Gourbilleau, *Int. J. Photoenergy* **2012**, *2012*, 1.

[3] G. Conibeer, M. A. Green, D. König, I. Perez-Wurfl, S. Huang, X. Hao, D. Di, L. Shi, S. Shrestha, B. Puthen-Veetil, Y. So, B. Zhang, Z. Wan, *Prog. Photovolt.* **2011**, *19*, 813.

[4] P. Lu, W. Mu, J. Xu, X. Zhang, W. Zhang, W. Li, L. Xu, K. Chen, *Sci. Rep.* **2016**, *6*, 22888.

[5] X. Pi, C. Delerue, *Phys. Rev. Lett.* **2013**, *111*, 177402.

[6] S. Zhou, X. Pi, Z. Ni, Y. Ding, Y. Jiang, C. Jin, C. Delerue, D. Yang, T. Nozaki, *ACS Nano* **2015**, *9*, 378.

[7] J. M. Luther, P. K. Jain, T. Ewers, A. P. Alivisatos, *Nat. Mater.* **2011**, *10*, 361.

[8] R. Demoulin, M. Roussel, S. Duguay, D. Muller, D. Mathiot, P. Pareige, E. Talbot, *J. Phys. Chem. C* **2019**, *123*, 7381.

[9] R. Guerra, S. Ossicini, *J. Am. Chem. Soc.* **2014**, *136*, 4404.

[10] K. Sakamoto, K. Nishi, F. Ichikawa, S. Ushio, *J. Appl. Phys.* **1987**, *61*, 1553.

[11] D. Hiller, J. López-Vidrier, S. Gutsch, M. Zacharias, M. Wahl, W. Bock, A. Brodyanski, M. Kopnarski, K. Nomoto, J. Valenta, D. König, *Sci. Rep.* **2017**, *7*, 8337.

[12] T. Philippe, F. De Geuser, S. Duguay, W. Lefebvre, O. Cojocaru-Mirédin, G. Da Costa, D. Blavette, *Ultramicroscopy* **2009**, *109*, 1304.

[13] A. S. Grove, O. Leistiko, C. T. Sah, *J. Appl. Phys.* **1964**, *35*, 2695.

[14] M. Fujii, K. Toshikiyo, Y. Takase, Y. Yamaguchi, S. Hayashi, *J. Appl. Phys.* **2003**, *94*, 1990.

[15] X. Hao, E. C. Cho, G. Scardera, E. Bellet-Amalric, D. Bellet, Y. Shen, S. Huang, Y. Huang, G. Conibeer, M. Green, *Thin Solid Films* **2009**, *517*, 5646.

[16] F. Vurpillot, A. Bostel, D. Blavette, *Appl. Phys. Lett.* **2000**, *76*, 3127.

[17] *Atom Probe Tomography: Put Theory into Practice* (Ed: W. Lefebvre-Ulrikson, F. Vurpillot, X. Sauvage), Academic Press, London **2016**.

[18] N. Garcia-Castello, S. Illera, J. D. Prades, S. Ossicini, A. Cirera, R. Guerra, *Nanoscale* **2015**, *7*, 12564.

[19] Z. Ni, X. Pi, S. Cottenier, D. Yang, *Phys. Rev. B* **2017**, *95*, 075307.

[20] K. I. Hunter, N. Bedford, K. Schramke, U. R. Kortshagen, *Nano Lett.* **2020**, *20*, 852.

[21] G. M. Dalpian, J. R. Chelikowsky, *Phys. Rev. Lett.* **2006**, *96*, 226802.

[22] A. Mimura, M. Fujii, S. Hayashi, K. Yamamoto, *Solid State Commun.* **1999**, *109*, 561.

[23] X. J. Hao, E. C. Cho, C. Flynn, Y. S. Shen, G. Conibeer, M. A. Green, *Nanotechnology* **2008**, *19*, 424019.

[24] Z. Ni, S. Zhou, S. Zhao, W. Peng, D. Yang, X. Pi, *Mater. Sci. Eng., R* **2019**, *138*, 85.

[25] T. Zhang, B. Puthen-Veettil, L. Wu, X. Jia, Z. Lin, T. C. J. Yang, G. Conibeer, I. Perez-Würfl, *J. Appl. Phys.* **2015**, *118*, 154305.

[26] B. Puthen Veettil, L. Wu, X. Jia, Z. Lin, T. Zhang, T. Yang, C. Johnson, D. McCamey, G. Conibeer, I. Perez-Würfl, *Appl. Phys. Lett.* **2014**, *105*, 222108.

[27] G. Cantele, E. Degoli, E. Luppi, R. Magri, D. Ninno, G. Iadonisi, S. Ossicini, *Phys. Rev. B* **2005**, *72*, 113303.

[28] X. D. Pi, R. Gresback, R. W. Liptak, S. A. Campbell, U. Kortshagen, *Appl. Phys. Lett.* **2008**, *92*, 123102.

[29] M. Dasog, G. B. De los Reyes, L. V. Titova, F. A. Hegmann, J. G. C. Veinot, *ACS Nano* **2014**, *8*, 9636.

[30] R. Wang, X. Pi, D. Yang, *J. Phys. Chem. C* **2012**, *116*, 19434.

[31] D. König, S. Gutsch, H. Gnaser, M. Wahl, M. Kopnarski, J. Göttlicher, R. Steininger, M. Zacharias, D. Hiller, *Sci. Rep.* **2015**, *5*, 9702.

[32] G. Thompson, M. Miller, H. Fraser, *Ultramicroscopy* **2004**, *100*, 25.